

Metamagnetic behavior in Fe₃Si and Fe₃Al

N.E. Christensen^{1,*}, J. Kudrnovský^{2,*}, C.O. Rodriguez^{3,♥}

¹) Department of Physics and Astronomy, University of Aarhus, DK-8000 Aarhus C, Denmark.

²) Institute ASCR, Na Slovance 2, CZ-18221 Prague 8, Czech Republic.

³) IFLYSIB, Grupo Física del Sólido, C.C. 565, La Plata, Argentina.

Abstract

The electronic properties of Fe₃Si and Fe₃Al in the cubic DO₃ structure are calculated within the local spin density approximation. There are two types of Fe atomic positions, one with tetrahedral symmetry ([A,C]) and one with cubic ([B]) point symmetry. The magnetic properties of the Fe[B] sublattice are similar to those of bcc iron (same symmetry), and this sublattice moment varies smoothly when the volume is varied. The [A,C] Fe atoms, on the other hand, exhibit magnetic phase transitions behavior when the volume is varied similar, and we refer to this as a *metamagnetic* behavior. The present calculations show that in Fe₃Si and Fe₃Al the transitions between various high-spin and low-spin phases are expected near and below the equilibrium volume, and experimental observation of the transitions should therefore be possible by means of high-pressure experiments.

Key words: Magnetism, electronic structure, iron compounds, pressure effects.

1. Introduction

Iron assumes in its ground state the body-centered cubic (bcc) structure and is ferromagnetic. This is also predicted by means of some *ab initio* calculations, but the total-energy results obtained in the numerically most accurate calculations using the local (Local Spin-Density Approximation, LSDA) approximation to the density functional theory [1-6] predict that the non-magnetic fcc structure should be more stable [7,8]. The energy minimum of the fcc phase is indeed close to that of bcc-Fe [8]. Further, it occurs at a volume where iron cannot form a spontaneous magnetisation. This is well known and may also be seen from a simple Stoner model [9]. The magnetic properties of fcc iron are nevertheless interesting because an expansion of the lattice not only causes the d-band narrowing required for fulfillment of the Stoner criterion for ferromagnetism, but the expanded fcc-Fe could assume several different magnetic states, high-spin and low-spin phases, when the volume is varied. This was, for example, demonstrated by the calculations by Kübler [10] and by Moruzzi et al. [11] This *metamagnetic* behavior can be explained within the LSDA Stoner theory [13-15], which was used by Krasko [16,17,8].

*) For correspondence, E-mail: nec@phys.au.dk.

*) For correspondence, E-mail: kudrnov@fzu.cz.

♥) For correspondence, E-mail: cor_ar@yahoo.com.

The LSDA-Stoner theory [14] is particularly simple to apply in cases where the spin densities can be assumed to be spherically symmetric inside the atomic spheres and where the wave functions at the Fermi level are dominated by one angular momentum component. In such cases, and the 3d transition metals belong to those, the Stoner parameter I , defined through the spin splitting (in a field H):

$$\Delta \epsilon(j, \vec{k}) \equiv \epsilon_{j\downarrow}^{\vec{k}} - \epsilon_{j\uparrow}^{\vec{k}} = 2\mu_B H + mI(j, \vec{k}), \quad (1.1)$$

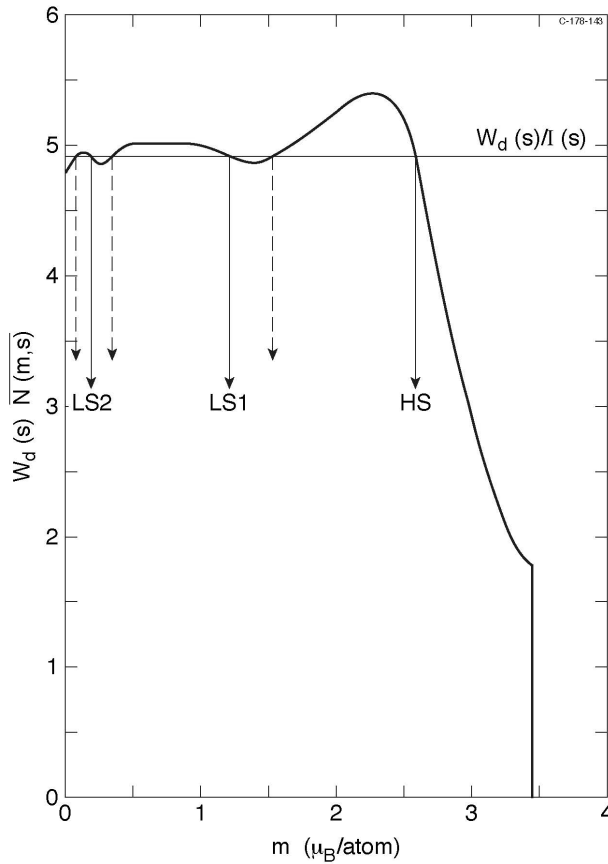
depends merely on energy, rather than being state dependent. Stoner parameters for the 3-d, 4-d, and 5-d series have been derived from atomic as well as spin polarised linear muffin tin orbital (LMTO) [18] band structure calculations [19,8]. If the density-of-states functions (DOS) for majority and minority spins can be assumed to have the same shape, then the magnetization m may be obtained by solving the Stoner equation:

$$I\bar{N}(m) = 1, \quad (1.2)$$

where

$$\bar{N}(m) \equiv m / (\epsilon_{\uparrow}(m) - \epsilon_{\downarrow}(m)) \quad (1.3)$$

is the DOS (per spin) averaged between the energies $\epsilon_{\uparrow}(m)$ and $\epsilon_{\downarrow}(m)$ defined by:



$$\frac{1}{2}m = \int_{\epsilon_F}^{\epsilon_{\uparrow}(m)} N(\epsilon) d\epsilon = \int_{\epsilon_{\downarrow}(m)}^{\epsilon_F} N(\epsilon) d\epsilon.$$

$$(1.4)$$

Here ϵ_F is the Fermi level in the non-polarised band structure.

Figure 1 illustrates the solution [16,17] of the Stoner type equation (1.2) for fcc iron. The DOS is dominated by the contribution from the d-states (3d), and we have applied a scaling by the d-band width, $W_d(S)$ (S is the Wigner-Seitz radius.) In this way the left-hand side of the equation

$$W_d(S)\bar{N}(m;S) = W_d(S)/I(S)$$

$$(1.5)$$

becomes essentially independent of the volume, and the right-hand side varies

(approximately) as S^{-5} .

Fig. 1: Graphical solution of the Stoner-like equation for fcc iron at a volume corresponding to the Wigner-Seitz radius $S = 2.70$ a.u. The density of states was derived from a local-density calculation for non-magnetic fcc-Fe using the LMTO method. Dashed arrows indicate unstable solutions, whereas LS1, LS2, and HS are stable low-spin and high-spin solutions (Refs 16,17).

We note that $I(S)$ is almost independent of S . This allows us to deduce the entire variation of m with volume from a single (non-polarized) band structure calculation. The result of such a calculation for fcc iron is shown in Fig. 2.

The metamagnetic behavior of fcc iron illustrated in Fig. 2 is interesting, but it should be noted that the equilibrium volume of Fe corresponds to $S = 2.54$ bohrs, a value that is far below those for which the LS and HS solutions can be found. Consequently, experimental observation of these phases would require substantial expansion of the lattice, and this would be very difficult to achieve. The body-centered iron, due to the shape of the bcc DOS, does not exhibit a similar magnetic multi phase structure. We have therefore looked for compounds of iron where the DOS shape could allow metamagnetism, and where this simultaneously would occur close to the equilibrium volume or under *compression*. The DO_3 structure of Fe_3Si and Fe_3Al has two types of Fe positions (see next section), one which is similar to that of bcc-Fe, and another more similar to fcc-Fe. The DOS related to the latter sublattice has a shape [20] that favors metamagnetic behavior. It is the purpose of the present paper to demonstrate this. Also, we shall examine similar effects in Fe_3Al .

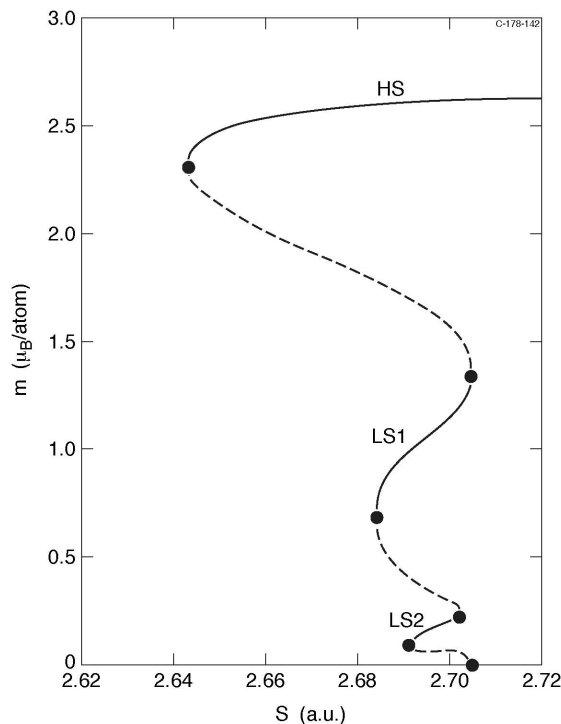


Fig. 2: LDA Stoner model for fcc Fe. The magnetic moment as a function of the Wigner-Seitz radius, S . The dashed lines indicate unstable solutions, whereas stable branches are shown with a full line. The equilibrium volume of fcc-Fe corresponds to $S = 2.54$ a.u.

The rest of the paper is organized as follows. Section 2 briefly describes the crystal structure and the non-polarized electronic structure of Fe_3Si . In Section 3 we report the result of full self-consistent LSDA calculations for Fe_3Si and Fe_3Al , and use the Stoner model to explain the metamagnetic behavior. A summary and a discussion follow in Section 4.

2. Crystal Symmetry and Band Structure of Fe₃Si

The ordered Fe₃Si and Fe₃Al crystallize in the DO₃ structure, see Fig. 3. It may be viewed as an fcc Bravais lattice with a basis consisting of four atoms, *A*, *B*, *C* and *D*, associated with each lattice point. For the compounds considered here, the *A* and *C* positions are both occupied with Fe, and these are equivalent, Fe[*A*]≡Fe[*C*]. Also the *B*-sublattice is occupied with iron atoms, Fe[*B*], whereas Si (or Al) occupy the *D* sites. Each Fe[*B*] atom is at the centre of a cube with four Fe[*A*] and four Fe[*C*] atoms at the corners. Thus Fe[*B*] is eightfold coordinated with the other Fe atoms, and the point symmetry is cubic. The nearest-neighbor environment seen by an Fe[*B*] atom is then just like in elemental bcc iron. Therefore we also found [20] that the magnetic moment of Fe[*B*] and the Fe[*B*]-DOS in Fe₃Si are very similar to those of bcc iron. The *A* and *C* sites have tetrahedral point symmetry with four Fe[*B*] and four Si[*D*] (or Al[*D*]) nearest neighbors.

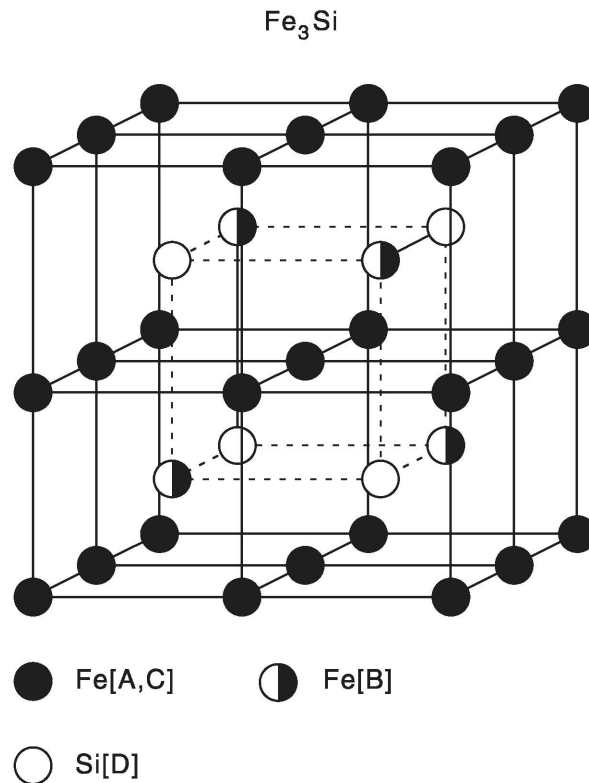


Fig. 3: Crystal structure of Fe₃Si.

This difference in symmetry of the two types of Fe positions causes important differences in the shapes of the site-projected DOS functions. Figure 2 in our earlier publication [20] shows that the Fe[*B*] DOS is characterised by having two main peaks (like bcc Fe), whereas the DOS associated with Fe[*A,C*] has a three-peak structure. In our earlier work, where Fe_{3-x}TM_xSi alloys (TM = transition metal) were examined, this difference was shown to explain the remarkable site preference observed for TM atoms substituting Fe in this type of compounds. Also, we compared *ab initio* calculations based on the LMTO-CPA (linear-

muffin-tin-orbital-coherent-potential approximation) method to the "local-environment model" used by Niculescu et al. [21].

The two-peak structure in the Fe[B] DOS really consists of three peaks. A low-lying t_{2g} peak is due to Fe[B]- d states bonding to the Fe[A,C] orbitals. The peak at the Fermi level (E_F) contains two peaks, the t_{2g} antibonding and an essentially non-bonding e_g peak. This picture was supported by [20] by calculation of partial DOS functions obtained from the states projected on cubic harmonics. Here it will be further illustrated by analysis of particular states in the band structure which is shown in Fig. 4. In the following discussion we number the bands from below in energy. The low-lying Fe[B] DOS peak is slightly below -2 eV, and at the zone centre (Γ) its major contribution comes from the the triply degenerate state (Γ'_{25}) formed by the bands 7-9. The non-bonding e_g state Γ'_{12} (bands 15-16 at Γ) is purely of Fe[B]- e_g character. But this state is almost coinciding in energy with the Fe[A,C] e_g state Γ_{12} (bands 13-14) which is antibonding to Fe[B]- d 's. The lowest triply degenerate state Γ_{15} (bands 2-4), is the Fe[A,C] bonding t_{2g} state. This gives only little eight to the Fe[B]-DOS. A similar analysis was carried out at other \mathbf{k} -points, but the one relating to the zone centre is sufficient to explain the features emphasized earlier [20].

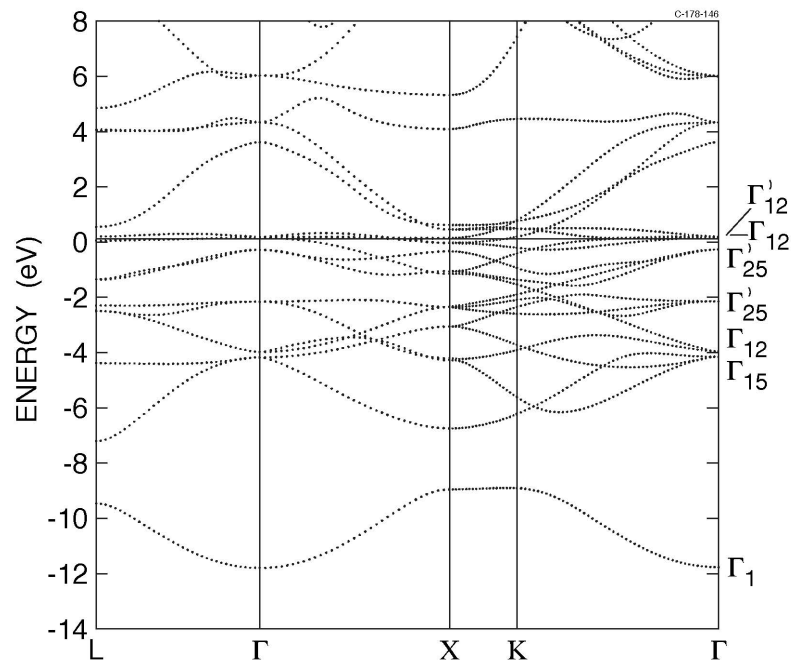


Fig. 4: Band structure of Fe_3Si (without spin polarisation). The lattice constant is 5.6548 Å (corresponding to an atomic-sphere radius of 2.6308 a.u.). The Fermi level, E_F , is at 0.120 eV.

We have here discussed the electronic structure of Fe_3Si , but it is interesting to note that this applies equally well to Fe_3Al , although Al has one electron less than Si. The peak in the DOS at E_F is so strong that it can pin the Fermi level even if the compound has one electron less on the D -site atom. The bonding properties remain essentially unchanged, and the crystal structure of Fe_3Al is the same as that of Fe_3Si . In view of this it is at first maybe surprising that the compounds Fe_3C and Fe_3B , which are completely *isoelectronic* with Fe_3Si and Fe_3Al do not form at ambient conditions in the cubic DO_3 structure. They prefer a more complicated orthorhombic structure, and this is presumably due to a difference in ionicity. The valence charge on the D site is clearly much larger in Fe_3C than in Fe_3Si as can be seen from Figs. 10 a and b. The reason is that C has no p core states whereas the $2p$ core states of Si, due to the orthogonality condition, prevent charge to flow into the D -site atomic region. This is also the

reason why the ionicity of SiC was found to be (surprisingly) large [22]. In Table 1 we list the excess number of electrons in the atomic spheres (space filling) calculated for the Fe₃X compounds. The structure was in all cases taken to be DO₃. Again we see that a large number of electrons accumulate on the [D] sites in the boride and the carbide. The volumes used in these calculations are the experimental values. One may choose to compare the charges by dividing space differently from what was done in the cases referred to in Table 1.

	S[a.u.]	N(Fe[A,C])	N(Fe[B])	N(X[D])
Fe ₃ C	2.505	- 0.2788	- 0.2262	0.7839
Fe ₃ B	2.533	- 0.2051	- 0.1696	0.5798
Fe ₃ Si	2.608	0.1691	- 0.0236	- 0.3146
Fe ₃ Al	2.695	0.1325	0.0677	- 0.3327

Table 1: Excess number of electrons, N, in the atomic spheres calculated for cubic (DO₃) Fe₃X, X= C, B, Si, Al. The Fe- and X spheres are chosen to be equal, and they are given by S in bohrs. (The atomic spheres are space filling, i.e. $16 \times 4\pi/3 S^3 = a^3$, where a is the lattice constant).

If we wish to compare Fe₃Si and Fe₃C at their respective equilibrium volumes, we may prefer to choose the Fe radii to be the same in the two cases, and then adjust the radii of Si and C so that the cell volumes are correct. With an Fe radius of 2.608 a.u., this implies that $S(\text{Si})=2.608$ a.u., and $S(\text{C})= 2.130$ a.u., i.e. substantially smaller than the value used in Table 1. (The average sphere radius in Fe₃C is still 2.505 a.u.). With this division the atomic spheres in Fe₃C are much closer to being neutral, Fe[A,C] has 0.063 extra electrons, and carbon lacks 0.034 electrons/atom in being neutral. But still, when we compare to the Fe₃Si charges in Table 1, the tendency of C to accumulate more valence electrons than Si is clear.

The total energies, see Table 2, as calculated by means of the full-potential LMTO method [23] confirm that Fe₃C prefer the orthorhombic to the cubic structure, and that Fe₃Si favors the DO₃ structure. The orthorhombic structure contains 4 formula units (16 atoms) in the primitive cell. The atomic positions are derived from the structural data for Fe₃C given by Wyckoff [24].

	Cubic	Orthorhombic
Fe ₃ C	- 2.6939	- 2.9143
Fe ₃ Si	- 2.7085	- 2.5764

Table 2: Total energies (Ry/formula unit) for Fe₃C and Fe₃Si calculated for the orthorhombic and cubic structures at the equilibrium volumes. Spin polarisation is not included. (Full-potential LMTO).

3. Magnetic Properties

Self-consistent LMTO calculations including spin polarization within the local spin-density approximation (LSDA) were performed for Fe₃Si and Fe₃Al for different volumes, and total energies and magnetic moments were derived. Figure 11 shows the calculated volume dependence of the total energy of Fe₃Al. The minimum occurs at the lattice constant $a_0^{\text{th}} = 5.718$ Å. The experimental^{25,27} equilibrium value is 5.791 Å, i.e. $\approx 1.5\%$ larger. Similar calculations for Fe₃Si yield $a_0^{\text{th}} = 5.606$ Å. This is $\approx 1\%$ smaller than the lattice constant, 5.65 Å, assumed by Niculescu et al. [21] and given in Pearson's handbook [25,26].

The moments obtained from the LSDA calculations at the equilibrium (theoretical) volumes are given in Table 3 where they also can be compared with experimental results [28-30].

The theoretical and experimental results agree reasonably well. The moments calculated for Fe₃Si agree particularly well with the neutron scattering data of Paoletti and Passani [28].

	Fe[A,C]	Fe[B]	Al/Si[D]
Fe ₃ Al theory	1.70	2.30	- 0.10
Fe ₃ Al expmt ^a	1.5 ± 0.10	2.18 ± 0.10	0.0
Fe ₃ Si theory	1.21	2.49	- 0.08
Fe ₃ Si expmt ^a	1.2 ± 0.12	2.4 ± 0.06	- 0.07 ± 0.06
Fe ₃ Si expmt ^b	1.07 ± 0.06	2.23 ± 0.06	
Fe ₃ Si expmt ^c	1.35	2.2	- 0.07

Table 3: Theoretical and experimental sublattice moments of Fe₃Al and Fe₃Si in Bohr magnetons (μ_B) per atom. a) Polarized neutron scattering [25], b) Polarized neutron scattering [29] and c) Saturation magnetization measurements [30].

The total energy variation in Fig. 5 shows that two self-consistent solutions were found for volumes somewhat below the equilibrium. They correspond to different ranges of the magnetic moments on Fe[A,C], high-spin (HS) and low-spin (LS). The separate iron moments in Fe₃Al as calculated by the self-consistent LSDA method are shown as functions of the volume in Fig. 6. The Fe[B] moment varies smoothly with volume. This is what we would expect since the point symmetry of Fe[B] is similar to that of bcc iron. The Fe[A,C] moments, on the other hand, vary strongly when the crystal is compressed, and multiple spin solutions exist ('metamagnetism'). The self-consistent calculations cannot converge in the regime of instability. We could have explored that regime by choosing a series of fixed values of the Fe[A,C]-*d* moments, $m_{Fe[A,C]}^d$, for each of these iterate to self-consistency to obtain the total energy $E_t(V, m_{Fe[A,C]}^d)$. The solution should then subsequently be obtained by determining the parameter values that minimize E_t . The calculated volume variation of the total moment in Fe₃Al is illustrated in Fig. 7, and Figs. 8-9 show the moments obtained for Fe₃Si. The metamagnetic behavior is also clearly seen in this case. A transition from a high-spin to a low-spin state is predicted to occur upon compression, and in Fe₃Si the pressure required is estimated to be 150-200 kbar.

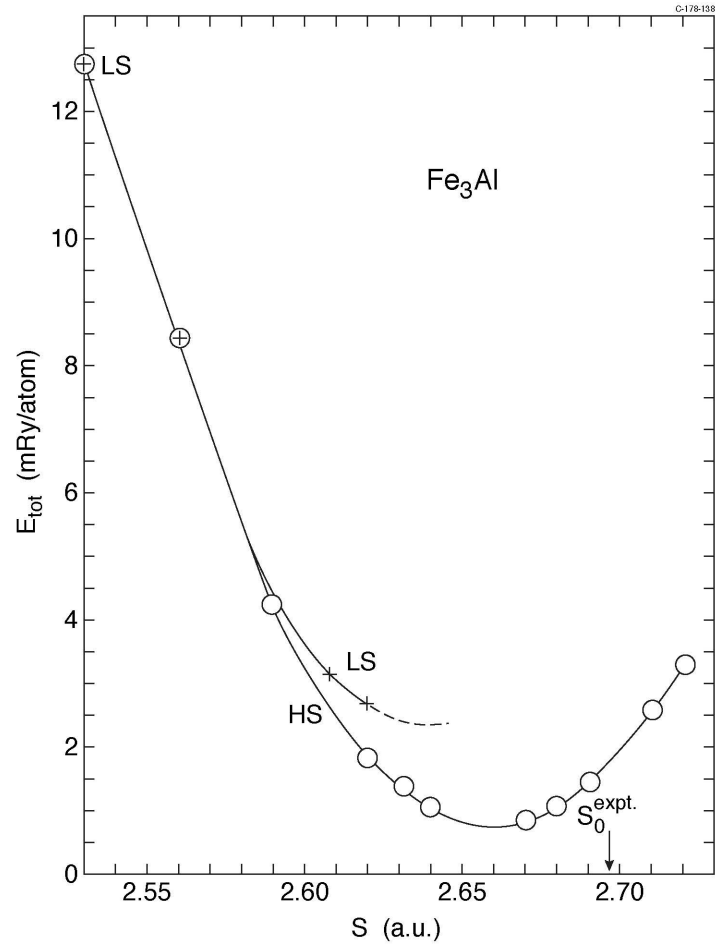


Fig. 5: Fe₃Al: Total energy (arbitrary zero offset) versus atomic-sphere radius. S_0^{expt} corresponds to the experimental^{25,27} lattice constant, $a_0 = 5.791$ Å. High-spin and low-spin phases are indicated by HS and LS, respectively.

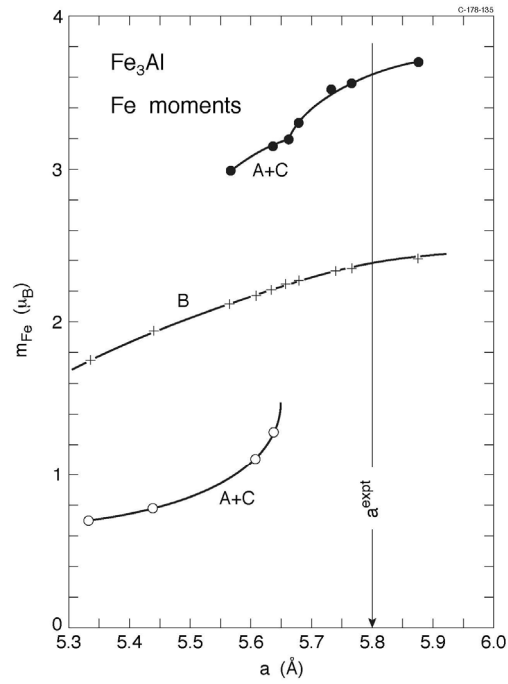


Fig. 6: Iron moments in Fe₃Al as obtained from self-consistent LSD calculations. The curves labeled A+C represent the sum of the Fe[A] and Fe[C] moments (which are equal), and B gives the Fe[B] moment. The experimental equilibrium lattice constant is indicated, a^{expt} .

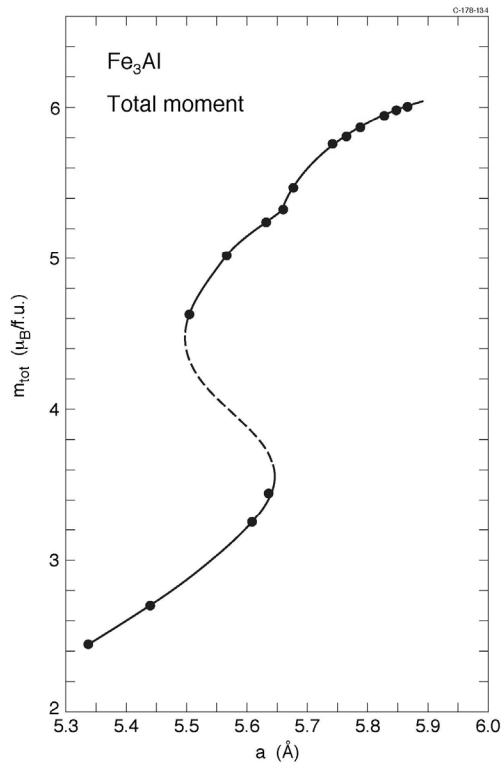


Fig. 7: Total moment in Fe₃Al as obtained from self-consistent LSD calculations. The dashed part sketches the instable regime (not calculated).

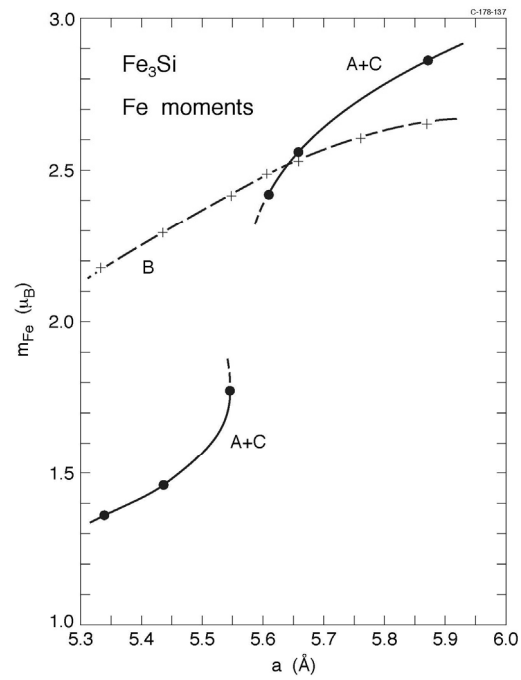


Fig. 8: Iron moments in Fe₃Si as obtained from self-consistent LSD calculations. The curves labeled A+C represent the sum of the Fe[A] and Fe[C] moments (which are equal), and B gives the Fe[B] moment.

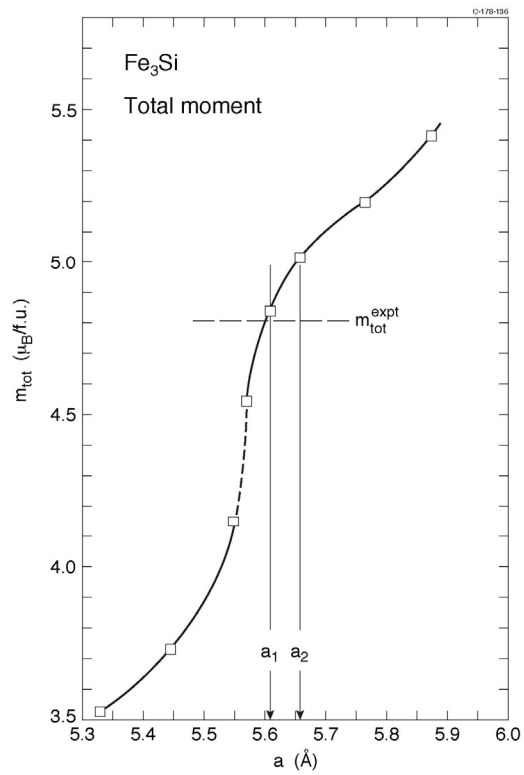


Fig. 9: Total moment in Fe_3Si as obtained from self-consistent LSD calculations. The dashed part sketches the instable regime (not calculated). The experimental lattice constant is a_2 , whereas the theoretical equilibrium volume corresponds to a_1 . The total moment as measured is indicated by m_{tot}^{exp} (from Ref. 21).

We can explain the metamagnetic behavior in terms of the Stoner model described in Section I. This was modified to treat the sublattices separately. Using the paramagnetic Fe[B] -DOS, no HS-LS transitions were found, as anticipated. But, as illustrated by Fig. 10, the A-C sublattice moment does exhibit metamagnetism. Although the sublattice Stoner model does not quantitatively fully reproduce the moments derived from the full self-consistent calculation, it does describe the existence of the various LS and HS states. The Stoner model assumed that the minority- and majority-spin DOS functions have the same shape as the density of states calculated without spin polarisation.

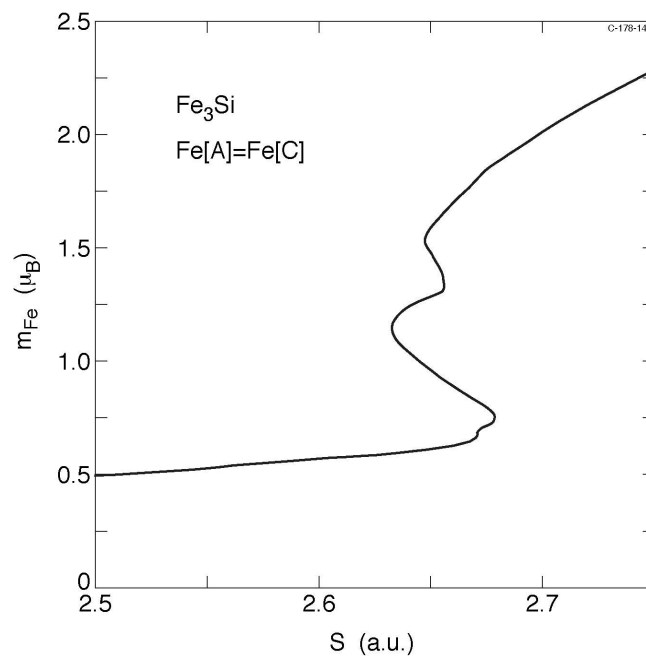


Fig. 10: Fe_3Si : Stoner model for the Fe[A,C] sublattice (see also Section I).

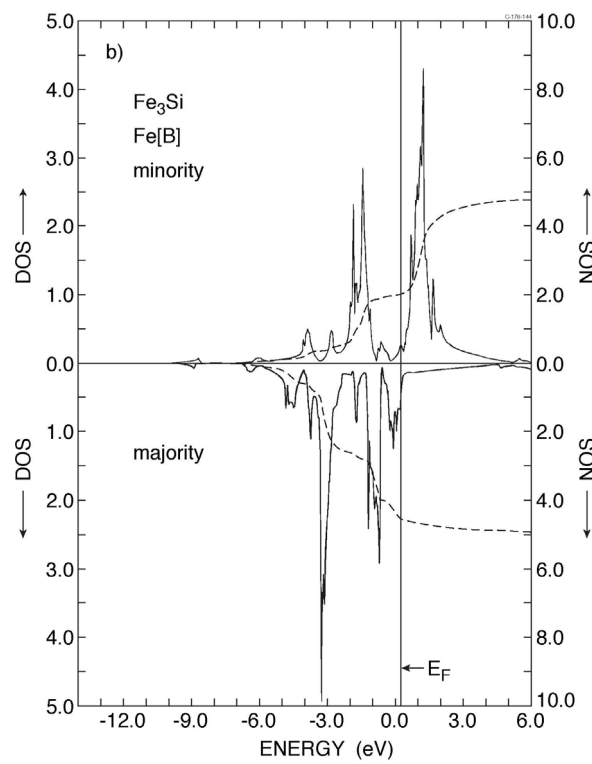
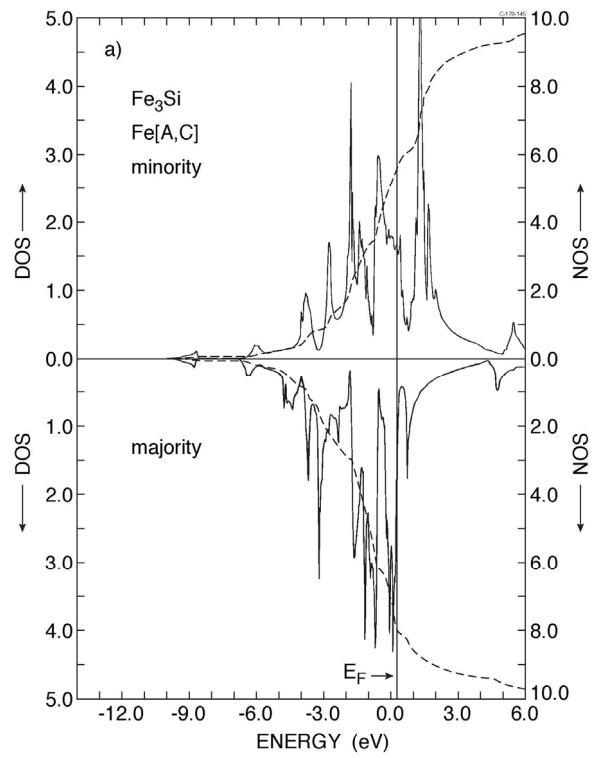


Fig. 11: Fe₃Si: Majority- and minority-spin density-of-states functions, DOS. The units are electrons per eV per atom. Figure a) is for Fe[A,C] and b) for iron on the B site. Same potential as in Fig. 12.

This assumption is not fully justified as can be seen from Fig. 11 which shows the DOS functions obtained from the full LSDA calculation for Fe₃Si. The gross features are similar in the \uparrow - and \downarrow -DOS, but some details are different. The band structure calculated for Fe₃Si with inclusion of spin polarization is shown in Fig. 12.

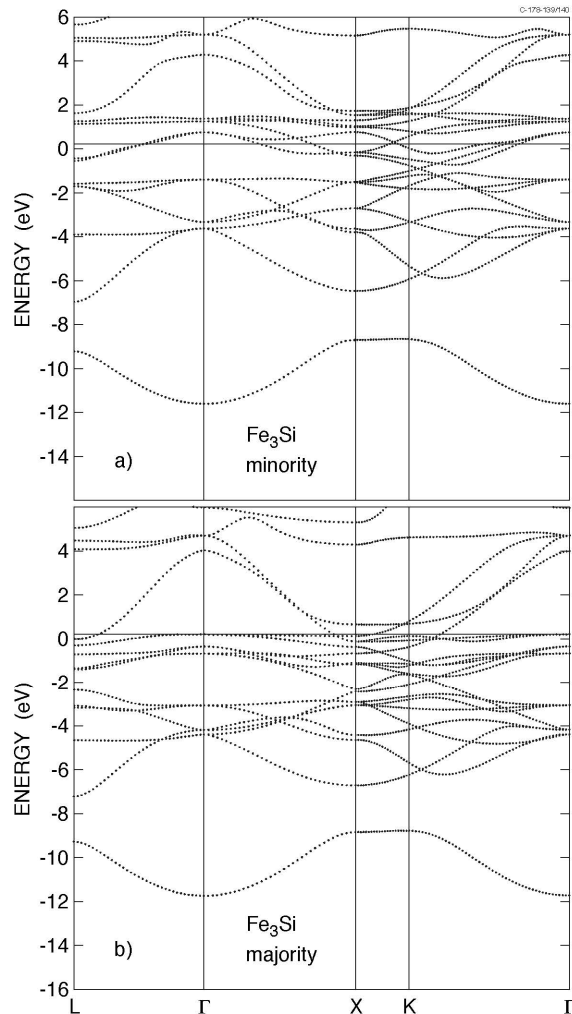


Fig. 12: Majority- and minority-spin bands structures calculated for Fe₃Si at the theoretical equilibrium volume ($a = 5.60 \text{ \AA}$, $S = 2.608 \text{ a.u.}$).

4. Summary and Discussion

First-principles electronic structure calculations for perfectly ordered Fe₃Si and Fe₃Al have been used to analyze the binding properties in the DO₃ structure. Total-energy calculations yield equilibrium lattice constants that are $\approx 1\text{-}1.5\%$ smaller than those observed. This reflects the tendency to overbinding when the LSDA is used in solid state calculations.

It is noted that the metallic compound Fe₃Si has an fcc Bravais lattice and the lattice constant is very close to that of GaAs. It might be of interest to examine metal-/semiconductor interfaces between these two materials.

The fact that Fe₃C and Fe₃B, although they are iso-valence-electronic with the two compounds otherwise studied here, do not form in the DO₃ structure is ascribed to a difference in ionicity. This is due to the lack of core-*p* electrons in C and B.

The different point symmetry of the [A,C] and [B] sites of the DO₃ structure explains the bonding as well as the different magnetic properties of Fe on these sublattices. The Fe[A,C] sublattice exhibits high-spin to low-spin transitions under compression, rather similar to what is predicted for fcc iron. But in contrast to the case of fcc Fe, the metamagnetic behavior in Fe₃Si (and Fe₃Al) should be accessible to experimental verification because compression relative to the ambient volume is required (in fcc iron a substantial expansion would be needed) to produce the major transition. A direct measurement of the magnetic moments as functions of applied pressure would be interesting. It is not straight-forward to perform polarized-neutron scattering experiments on a sample in a diamond anvil cell, but such measurements have been done on other materials [31]. One might also expect the optical properties to change so that the transition could be detected by measuring the reflectivity under pressure. K. Syassen and his collaborators in Stuttgart [32] did perform reflectivity measurements on Fe₃Si for pressures up to 300 kbar. The photon energy range was 0.5-4.0 eV. Except for a change in the absolute reflectivity by $\Delta R = 0.1$ near 100 kbar hardly any change was seen up to 300 kbar. The structure in the spectra is weak, but a shift of one shoulder by ≈ 0.3 eV near 120 kbar might be present. Nevertheless, the data do not unambiguously show the transition predicted. Further experiments are required and, not less important, we must calculate the optical spectra in order to estimate the effects of the HS-LS transitions on the optical properties.

References

- [1] P. Hohenberg, W. Kohn, Phys.Rev. B **136** (1964) 964
- [2] W. Kohn, L. J. Sham, Phys. Rev. A **140** (1965) 133
- [3] L. J. Sham, W. Kohn, Phys. Rev. **145** (1966) 561
- [4] U. von Barth, L. Hedin, J. Phys. Colloq. France **33** (1972) C5-1629
- [5] S. H. Vosko, L. Wilk, M. Nusair, Can. J. Phys. **58** (1980)1200
- [6] O. Gunnarsson, B. I. Lundqvist, Phys. Rev. B **13** (1976) 4274
- [7] C. S. Wang, B. M. Klein, H. Krakauer, Phys. Rev. Lett. **54** (1985)1852
- [8] N. E. Christensen, O. Gunnarsson, O. Jepsen, O. K. Andersen, Journ. de Physique, Coll. C8, Suppl. to No. 12, Vol. **12** (1988) C8-17
- [9] U. K. Poulsen, J. Kollár, O. K. Andersen, J. Phys. F **6** (1976) L241
- [10] J. Kübler, Phys. Lett. A **81** (1981) 81
- [11] V. L. Moruzzi, Phys. Rev. Lett. **57** (1986)2211
- [12] V. L. Moruzzi, P. M. Marcus, K. Schwarz, P. Mohn, Phys. Rev. B **34** (1986) 1784
- [13] S. H. Vosko, J. L. Perdew, A. H. MacDonald, Phys. Rev. Lett. **35** (1975)1725
- [14] O. K. Andersen, J. Madsen, U. K. Poulsen, O. Jepsen, J. Kollar, Physica **86-88B** (1977) 247
- [15] O. Gunnarsson, J. Phys. F **6** (1976) 587
- [16] G. L. Krasko, N. E. Christensen, unpublished (1986)
- [17] G. L. Krasko, Phys. Rev. B **36** (1987) 8565
- [18] O. K. Andersen, Phys. Rev. B **12** (1975) 3060
- [19] O. K. Andersen, O. Jepsen, D. Glötzel, in *Highlights of Condensed Matter Theory*, eds. F. Bassani, F. Fumi, and M. P. Tosi (North-Holland, Amsterdam) p. 59,1985
- [20] J. Kudrnovský, N. E. Christensen, O. K. Andersen, Phys. Rev. B **43** (1991)5924

- [21] A. Niculescu, T. J. Burch, J. I. Budnik, J. Magn. Mater. **39** (1983)223
- [22] N. E. Christensen, S. Satpathy, Z. Pawlowska, Phys. Rev. B **36** (1987)1032
- [23] M. Methfessel, Phys. Rev. B **38** (1988)1537
- [24] R. W. G. Wyckoff, *Crystal Structures*, Second edition, John Wiley & Sons, New York (1967)
- [25] '*Pearson's Handbook of Crystallographic Data for Intermetallic Phases*', edited by P. Villars and L. D. Calvert, ASM International, Materials Park (OH) (1991)

- [26] S. N. Mishra, D. Rambabu, A. K. Grover, R. G. Pillay, P. N. Tandon, H. G. Devare, R. Vijayaraghavan, J. Appl. Phys. **57** (1985) 3258
- [27] Popiel, M. Tuszynski, W. Zarek, T. Rendecki, J. Less-Common Metals **146** (1989) 127
- [28] A. Paoletti, L. Passani, Nuovo Cimento **32** (1964) 1449
- [29] J. Moss, P. J. Brown, J. Phys. F **2**, (1972) 358
- [30] W. A. Hines, A. H. Menotti, J. I. Budnik, T. J. Burch, T. Litrenta, V. Niculescu, K. Raj, Phys. Rev. B **13** (1976) 4060
- [31] J. M. Besson, R. J. Nelmes, J. S. Loveday, G. Hamel, Ph. Pruzan, S. Hull, High Pressure Research **9** (1992)179
- [32] K. Syassen, private communication (unpublished).